JHEP|Reports

Modeling of hepatitis B virus kinetics and accumulation of cccDNA in primary human hepatocytes

Authors

Louis Shekhtman, Yuji Ishida, Masataka Tsuge, …, Susan L. Uprichard, Harel Dahari, Kazuaki Chayama

Correspondence

chayama@mba.ocn.ne.jp (K. Chayama), hdahari@luc.edu (H. Dahari).

Graphical abstract

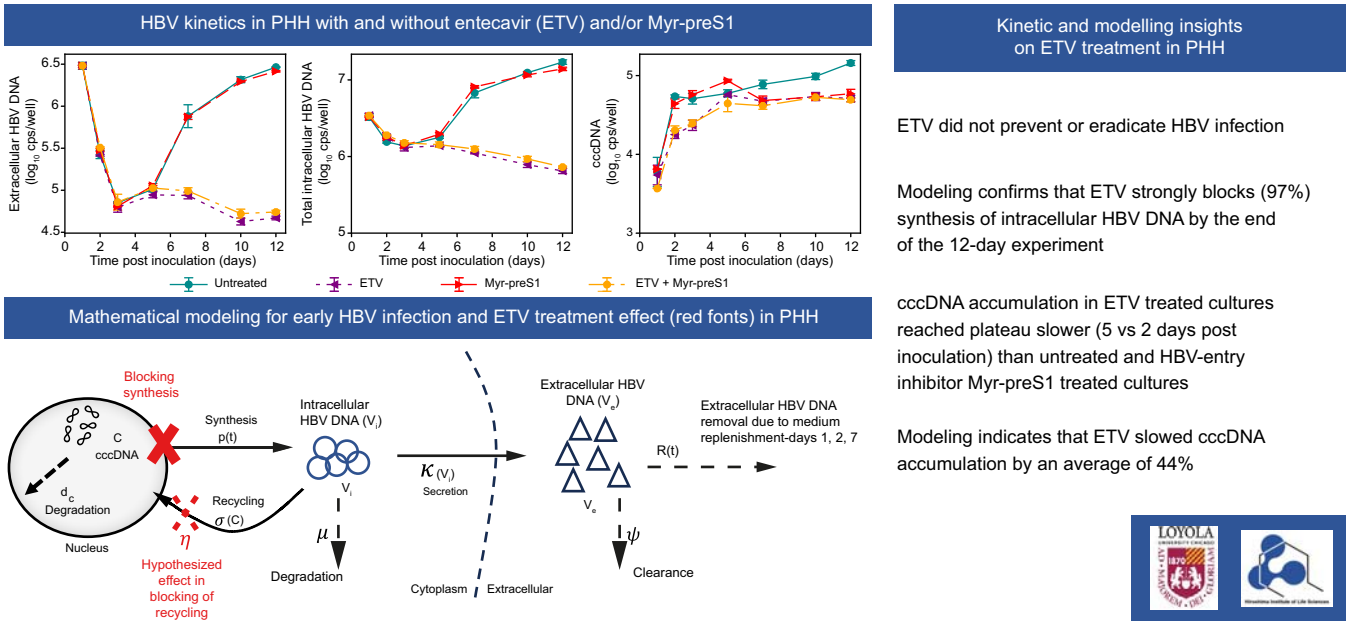

Highlights:

- Longer viability of PXB cells compared with standard PHHs enables a more detailed HBV kinetic characterization post infection.
- Mathematical modeling confirms that entecavir strongly blocks (97%) the synthesis of intracellular HBV DNA accumulation.
- Modeling predicts that entecavir slows cccDNA accumulation by 44% without affecting the final cccDNA plateau level.
- Entecavir may have a multifunctional antiviral effect delaying cccDNA accumulation.

Impact and implications:

Using primary human hepatocytes (PHHs), we characterize early HBV kinetics post infection. HBV-infected PHH were treated with an entry inhibitor to characterize the accumulation of intracellular and extracellular HBV DNA and the nuclear episomal viral genome called covalently closed circular DNA (cccDNA) in the absence of HBV spread. Kinetic and mathematical modeling in PHHs confirms that the replication inhibitor, entecavir, strongly blocks intracellular HBV DNA accumulation, which also slowed the accumulation of cccDNA. However, modeling indicates that effects on cccDNA accumulation are not directly determined by intracellular HBV DNA levels, supporting the conclusion that cccDNA levels within the cell are regulated in some yet-to-be-elucidated manner.

https://doi.org/10.1016/j.jhepr.2024.101311

Research article

JHEP|Reports

Modeling of hepatitis B virus kinetics and accumulation of cccDNA in primary human hepatocytes

Louis Shekhtman[1,2,†], **Yuji Ishida**[3,†], Masataka Tsuge[4,5], Vladimir Reinharz[6], Mikaru Yamao[3], Masaki Takahashi[3], Chise Tateno[3], Susan L. Uprichard[1], Harel Dahari[1,*], Kazuaki Chayama[7,8,*]

JHEP Reports **2025**. vol. 7 | 1–8

Background & Aims: Knowledge about early HBV covalently closed circular DNA (cccDNA) accumulation post infection is lacking. We characterized and mathematically modeled HBV infection kinetics during early infection and treatment in primary human hepatocytes (PHHs).

Methods: PHHs were inoculated with HBV, and infection was monitored with and without treatment with the nucleoside analog entecavir (ETV), the HBV-entry inhibitor Myr-preS1, or both ETV + Myr-preS1. Extracellular HBV DNA (exHBV), total intracellular HBV DNA (inHBV), and cccDNA were frequently measured during the 12 days post inoculation. A multicompartmental mathematical model was developed to explain HBV infection dynamics.

Results: Multiphasic exHBV and inHBV kinetics were overall similar in untreated and Myr-preS1-treated PHHs. In ETV-treated PHHs (either alone or with Myr-preS1), exHBV and inHBV initially declined and did not resurge. ETV-treated cultures had significantly (p=0.002) lower mean cccDNA levels at Day 2 post inoculation (4.3 ± 0.1 *vs*. 4.7 ± 0.1) and reached plateau slower (5 *vs*. 2 days) than untreated and Myr-preS1-treated cultures, respectively. Modeling predicts that the recycling of inHBV into cccDNA stops when cccDNA reaches a maximum and HBV secretion changes depending on the concentration of inHBV. Even when initiated at the time of inoculation, ETV did not prevent or eradicate infection but rather blocked inHBV accumulation gradually, reaching 97% efficacy by the end of the 12-day experiment and resulting in an average 44% slower cccDNA accumulation.

Conclusions: The study provides insight into the interrelationships and dynamics of cccDNA accumulation, inHBV accumulation, and secretion of exHBV containing particles. Although kinetics and modeling support the conclusion that the level of cccDNA in the cell is regulated, the mechanisms that determine HBV capsid secretion *vs*. recycling to the nucleus for cccDNA accumulation require further investigation.

Introduction

Hepatitis B Virus (HBV) infection is a serious global health problem, with ∼254 million people worldwide chronically infected, causing more than 1,100,000, deaths per year.[1] Current antiviral therapies using nucleoside/nucleotide analogs (NAs) and/or interferon can suppress HBV replication but are rarely able to achieve complete elimination of HBV because of their inability to eradicate the episomal nuclear DNA pools in hepatocytes known as covalently closed circular DNA (cccDNA).[2] To support current efforts toward developing HBV cures,[3] it is crucial to understand HBV infection dynamics at the molecular level.

A key aspect of HBV infection is the accumulation and maintenance of cccDNA in the nucleus, from which viral genes are expressed as well as the pregenomic RNA template necessary for the first step in synthesizing intracellular HBV DNA (inHBV). Once partially double-stranded, the encapsidated inHBV can then either be enveloped and secreted out of the cell or be recycled back to the nucleus to be converted to cccDNA. The kinetics and mechanisms through which cccDNA levels accumulate during infection initiation as well as how cccDNA levels are maintained during chronic infection (i.e. recycling *vs*. *de novo* infection) remain to be fully understood. Treatment with a myristoylated pre-S/2-48myr peptide (Myr-preS1), which binds to the cellular NTCP receptor, inhibits HBV entry into cells, preventing HBV spread.[4,5] Furthermore, there has been interest in whether Myr-preS1 might affect cccDNA levels as a result.[5,6]

Another treatment, entecavir (ETV), is one of the most effective NAs commonly used to treat HBV.[7] Although ETV treatment can suppress serum HBV DNA levels to undetectable levels[8] and has been shown to reduce cccDNA over time,[9] long-term therapy rarely achieves elimination of cccDNA.

* Corresponding authors. Addresses: Hiroshima Institute of Life Sciences, Hiroshima, Japan. Tel.:+81-82-236-7613; Fax: +81-82-236-7614 (K. Chayama); The Program for Experimental and Theoretical Modeling, Division of Hepatology, Department of Medicine, Stritch School of Medicine, Loyola University Chicago, Maywood, IL, USA. Tel.: +1-708-216-4682; Fax: +1-708-216-6299 (H. Dahari).
E-mail addresses: chayama@mba.ocn.ne.jp (K. Chayama), hdahari@luc.edu (H. Dahari).
† Louis Shekhtman (theoretical [in silico] work) and Yuji Ishida (experimental [in vitro] work) contributed equally to this study.
https://doi.org/10.1016/j.jhepr.2024.101311

Moreover, although much focus has been placed on the low levels of resistance to ETV, minimal prior work[10] has explored ETV treatment during acute infection and how ETV affects cccDNA dynamics.

Mathematical models of HBV infection have been useful for understanding the dynamics of infection and elucidating the underlying biological features involved. Although most of these modeling efforts have not focused on intracellular HBV dynamics, several have. Murray *et al.*[11] developed an intracellular mathematical model to investigate the dynamics of infection and clearance in three acutely infected immunocompetent chimpanzees with weekly sampled data. Several other works studied *in silico* models that provided insights into HBV replication dynamics.[12,13] A very recent work considered a model that included cccDNA but did not focus on early accumulation of cccDNA or early infection dynamics in general.[14] Hence, understanding early HBV infection *in vitro* using intracellular mathematical models is lacking.

Here, we develop a multicompartment mathematical model to provide insights into the early dynamics of HBV infection and treatment *in vitro* in primary human hepatocytes (PHHs). The model comprises three compartments: cccDNA in the nucleus, total inHBV, and extracellular HBV DNA (exHBV) in media. It is worth mentioning that the media outside the cell must be replenished at multiple time points during the experiment, leading to routine removal of the exHBV. Our data-driven modeling approach incorporates these media changes so that insights can be derived despite necessary routine perturbations to the system.

Materials and methods

Preparation of PHHs

PHHs were prepared as described previously.[15] Briefly, commercially available cryopreserved human hepatocytes (lot 195 [BD Bioscience], Hispanic, female, 2 years; lot JFC [BIO-IVT], Caucasian, male, 1 year; and lot TNX [BIO-IVT], Caucasian, female 8 months) were transplanted in cDNA-uPA/SCID mice via the spleen. PHHs were isolated from the chimeric mice with humanized livers at 9–15 weeks after transplantation by standard collagenase perfusion. Regarding lot BD195, the isolated PHHs were serially transplanted into cDNA-uPA/SCID mice for subsequent amplification. Nine to 15 weeks after the serial transplantation, PHHs were collected and seeded on type I collagen-coated 24-well plates (4.0×10^5 cells/well) for experiments. PHHs were cultured *in vitro* with 500 μl of 2% DMSO-supplemented hepatocyte clonal growth medium under 5% CO_2 and 95% air at 37 °C. Notably, the PHHs derived here from the uPA/SCID mice are a well-established PHH-based model known to accurately recapitulate results from human liver-derived PHHs.[16–18]

All animal protocols described in this study were performed in accordance with the Guide for the Care and Use of Laboratory Animals and approved by the Animal Welfare Committee of Phoenix Bio Co, Ltd. (Hiroshima, Japan).

Preparation of HBV stocks

The original serum samples were obtained from patients infected with HBV genotype C (from Nagoya City University [AB246345]) after obtaining written informed consent for the donation and evaluation of blood samples. Serum was positive for HBsAg and HbeAg with high-level viremia. The experimental protocol meets the ethical guidelines of the Declaration of Helsinki and was approved by the Ethical Committees of Hiroshima University and Nagoya City University. Serum was injected into human hepatocyte chimeric mice via the mouse tail vein. After the inoculated mice reached high viremia, mouse serum was collected and stored at -80 °C until use.

HBV infection

PHHs were inoculated with HBV as previously described[19] with 5 or 10 genome equivalents (GEq)/cell for 1 day in the presence of 4% polyethylene glycol (PEG) 8000. ETV treatment (2.5 nM or 10 μM) was started in parallel with the viral inoculum. MyrpreS1 treatment (6.25 μg/ml) was initiated 1 day post inoculation (p.i.). During the experiments, culture media was renewed at 1, 2, and 7 days after HBV inoculation. The drug treatments were continued throughout infection, and all experiments were performed in triplicates. Culture media was collected at 1, 2, 3, 5, 7, 10, and 12 days after HBV inoculation in experiment 1 (frequent HBV kinetic experiment). In the infrequent HBV kinetic experiment (experiment 2), the culture media was collected at 3, 7, and 12 days after HBV inoculation. In experiments 3, 4, and 5, we used different PXB-cell donors and performed HBV inoculation with or without ETV, where culture media was collected at 1, 2, 7, and 12 days after HBV inoculation. HBV genotype C was used in all experiments.

Quantification of HBV DNA and HbsAg in the culture medium

DNA was extracted from the culture media or cells using the SMITEST EX-R&D Nucleic Acid Extraction Kit (Medical & Biological Laboratories Co, Ltd., Nagoya, Japan). inHBV, exHBV, and cccDNA HBV levels were quantified by quantitative real-time PCR (qPCR) as previously described.[19–21] Total exHBV and cccDNA qPCR was performed using 100 ng of extracted DNA extract. HbsAg was quantified by ELISA, as previously described.[19,22]

Statistical analysis

All statistical analysis were performed using Python (version 3.11) and packages scipy (version 1.3) and numpy (version 1.17). Results with p values ≤0.05 were considered statistically significant. The phase-wise slopes (with 95% CIs) of exHBV, HbsAg, inHBV, and cccDNA were estimated using linear regression.

Mathematical model

We developed a multicompartment mathematical model to provide insights into the early dynamics of HBV during infection and treatment in PHHs (Fig. 1). The model comprises three compartments per well: cccDNA (C) in the nucleus, total inHBV (V_i), and exHBV (media) (V_e). The cccDNA (C) equation is as follows:

$$\frac{dC}{dt} = \eta\sigma(C)V_i - d_cC, \quad (1)$$

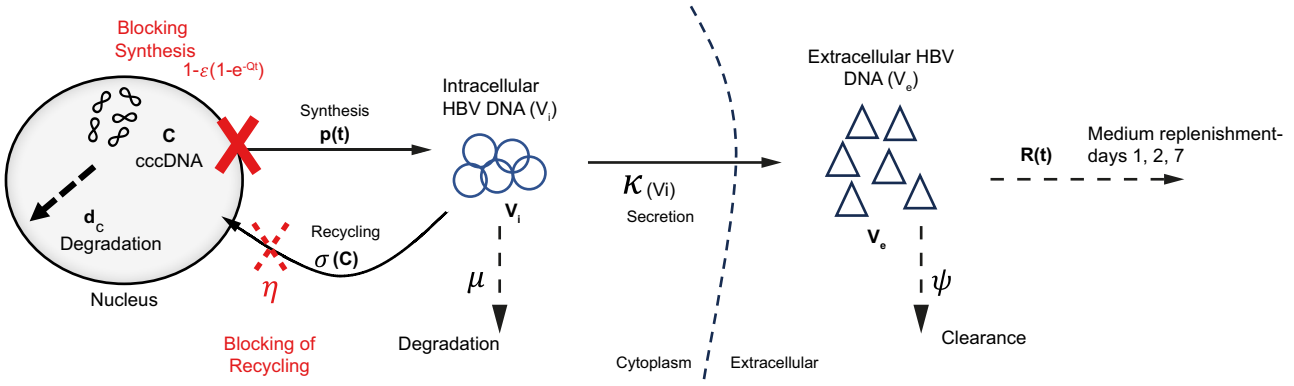

Fig. 1. Schematic diagram for the HBV replication mathematical model in PHHs. The left side of the dashed line represents intracellular space, and the right side represents extracellular space. During the infection, HBV enters into the cell and releases protein envelope into the cytoplasm of PHHs. After uncoating the HBV virions into the cytoplasm, the partially double-stranded DNA is transported to the nucleus, where its genomic relaxed circular DNA forms cccDNA *C* (figure-eight symbols), which degrades with rate constant d_c. *C* is synthesized to iHBV (V_i, circles) at rate $p(t)$, and V_i degrades at the rate constant (μ). iHBV is assembled/secreted from cell as eHBV (V_e, triangles) at the rate ($\kappa(V_i)$). V_e degrades with the rate constant ψ. A fraction of the iHBV DNA re-imports back to form cccDNA copies with the recycling rate ($\sigma(C)$). In the experiment, the medium was replenished at Days 1, 2, and 7. ETV effects (red) block the synthesis of V_i by a fraction (1 - ε) and has a secondary hypothesized effect (dashed X) of reducing recycling of iHBV by a fraction η. cccDNA, covalently closed circular DNA; ETV, entecavir; exHBV, extracellular HBV DNA; inHBV, intracellular HBV DNA; PHH, primary human hepatocyte.

$$\sigma(C) = \sigma_{max}\left(1 - \frac{C}{C_{max}}\right),$$

where σ(*C*) is the cccDNA-dependent logistic growth rate, σ_{max} is the maximum recycling rate, C_{max} is the maximum level of cccDNA per well at which cccDNA accumulation stops, and d_c is the degradation rate constant of cccDNA. *t* represents the time since HBV inoculation. As shown in Fig. 2, cccDNA accumulation is slower in the presence of ETV and ETV + Myr-preS1 compared with cells not treated with ETV. Parameter η modifies $\sigma(C)$ to account for this effect ($0 \le \eta < 1$).

The total inHBV (V_i) equation is as follows:

$$\frac{dV_i}{dt} = \left(1 - \varepsilon\left(1 - e^{-(Q*t)}\right)\right)p(t)C - \kappa(V_i)V_i - (\sigma(C) + \mu)V_i, \quad (2)$$

$$p(t) = \frac{p_{max}}{(1+e^{-m(t-\tau)})} \quad \text{and} \quad \kappa(V_i) = \begin{cases} 0, & \text{if } t<\tau_1 \\ \dfrac{\kappa_{max}V_i^n}{V_{i50}^n + V_i^n}, & \text{if } t \ge \tau_1 \end{cases}$$

where V_i is produced at rate $p(t)C$, $p(t)$ is the time-dependent V_i synthesis rate, p_{max} is the maximum synthesis constant rate, τ is the time to reach approximately 50% of p_{max}, and *m* governs the increase to p_{max}. For simplicity, we do not distinguish between multiple intracellular replication steps such as the generation of cytoplasmic capsid assembly or the generation of HBV single-stranded DNA by reverse transcription and maturation to double-stranded DNA inside the capsid. V_i is degraded with rate constant μ, recycled to the nucleus at rate $\sigma(C)V_i$, and enveloped/secreted at rate $\kappa(V_i)V_i$. $\kappa(V_i)$ was modeled using a Hill function, where κ_{max} is the maximum secretion rate constant, V_{i50} is the level

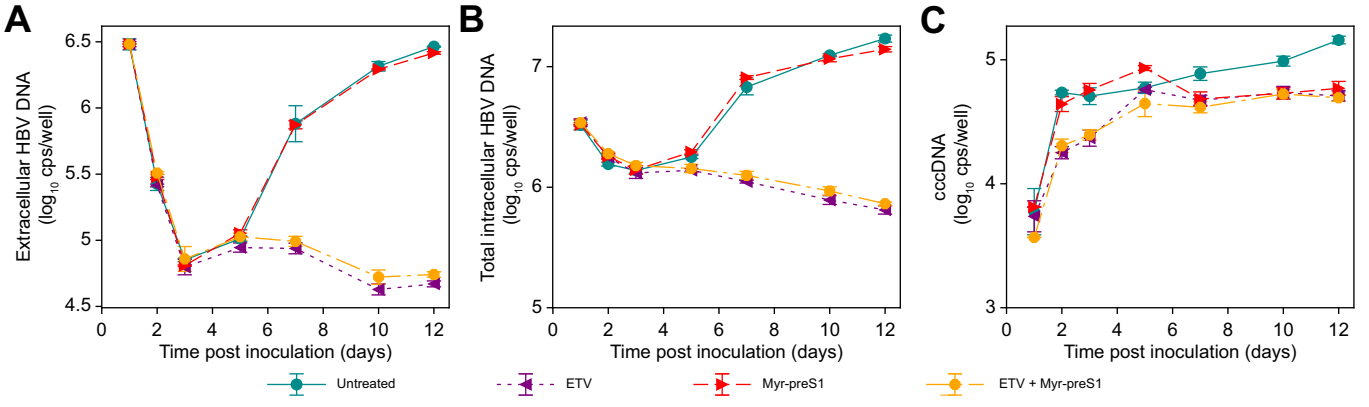

Fig. 2. HBV kinetics during infection and treatment. PHHs were inoculated with 10 GEq/cell HBV. Cultures were either left untreated (UT) or treated with ETV, Myr-preS1, or ETV + Myr-preS1. Three samples were harvested at the indicated time points,and HBV DNA was quantified by qPCR. (A) Extracellular HBV DNA, (B) total intracellular HBV DNA, and (C) cccDNA. Data is graphed as mean ± SD. cccDNA, covalently closed circular DNA; ETV, entecavir; GEg, genome equivalents; inHBV, intracellular HBV DNA; Myr-preS1, myristoylated pre-S/2-48myr peptide; PHH, primary human hepatocyte; qPCR, quantitative real-time PCR.

of V_i at which the secretion rate reaches half of κ_{max}, and n is the Hill coefficient. Because there is a delay in synthesis of inHBV, we assume that there is no virion secretion (κ = 0) before time τ_1. ETV reduces the V_i synthesis rate with a time-dependent efficacy of $(1 - \varepsilon(1 - e^{-Qt}))$.

The exHBV (V_e) equation is as follows:

$$\frac{dV_e}{dt} = \kappa(V_i)V_i - \psi V_e - R(t), \quad (3)$$

$$R(t) = \begin{cases} 0 & \text{if } t<1 \\ V_e\mu e^{-\lambda(t-1)} & \text{if } t\geq 1 \\ V_e\mu\left(e^{-\lambda(t-1)}+e^{-\lambda(t-2)}\right) & \text{if } t\geq 2 \\ V_e\mu\left(e^{-\lambda(t-1)}+e^{-\lambda(t-2)}+e^{-\lambda(t-7)}\right) & \text{if } t\geq 7 \end{cases},$$

where V_e is produced at rate $\kappa(V_i)$ V_i and cleared with constant rate ψ. Media replenishment at Days 1, 2, and 7 is modeled using $R(t)$ as an exponential decay function, where ν is the exHBV decline resulting from replenishment and λ is the exponential decay constant.

Parameter estimations

HBV DNA stability in media (ψ)

To estimate exHBV (V_e) degradation rate ψ, culture media at 12 days p.i. were collected into microcentrifuge tubes, which were pretreated with a culture medium containing 10% of FBS for 10 min. Samples were incubated at 37 °C for 1 and 5 days. After the incubation, HBV DNA levels were quantified by qPCR as described above and were found to be stable (Table S1.3). Therefore, a clearance rate that is not significant was assumed over the period considered, and we chose to set ψ = 0.012 per day (*i.e.* $t_{1/2}$ = 57 days), a half-life that is much longer than the period of our experiment.

cccDNA degradation rate (d_c)

The half-life ($t_{1/2}$) of cccDNA has been assumed to be on the order of weeks to months.[10,23,24] Because the 12-day experiment is too short to estimate cccDNA $t_{1/2}$ in PHHs, d_c was fixed at 0.01/day (*i.e.* $t_{1/2}$ = 69 days).

Fixing parameters because of identifiability issues

Because parameters m and τ (Eq. 2) are coupled and cannot be individually estimated, m was arbitrarily fixed at 1.5. Because of identifiability issues, for simplicity, n was fixed at 1, and V_{i50} was fixed at 5×10^6 cps/well. As noted in the Supplementary information, λ was fixed at 4.2 because of high uncertainty, with the value of 4.2 arising from initially setting the value to 4.7, fitting all other parameters and then determining the best value of λ. Likewise, selecting values from λ = 3 to 5 tends to provide a good fit.

Initial conditions

The initial values of inHBV and exHBV for model calibration are given by mean baseline measured data at Day 1 for untreated (or ETV-treated) PHHs. The initial inHBV and exHBV values were $V_{i0} = 3.35 \times 10^6$ cps/well and $V_{e0} = 3 \times 10^6$ cps/well, respectively. The initial value of cccDNA was assumed to be C_0 = 0 cps/well.

Estimation of unknown parameters

Estimation of initiation of productive HBV infection. To account for the time between inoculation and the moment the virus enters PHHs to establish infection (which is the initial time to start the model), we introduced parameter S_0, which was constrained between 0 and 1 because the HBV kinetic data were measured from Day 1 pi.

The remaining parameters, S_0, σ_{max}, C_{max}, τ, p_{max}, κ_{max}, τ_1, μ, ν, ε, η, and Q were estimated via model calibration that was implemented in Python 3.11. To solve the model, the integrate.solve_ivp method from Virtanen *et al.*[25] was used, with the Explicit Runge–Kutta method of order 5(4). Parameter fitting was performed using the lmfit library[26] and the Levenberg–Marquardt algorithm. The standard deviations were computed from the returned correlation matrix. The model was simultaneously calibrated on total exHBV, total inHBV, and cccDNA first to obtain fits for parameters that are not related to treatment with ETV. For this purpose, the Myr-preS1-treated cells were used and fitted to avoid any effects of potential spread, as suggested by statistically significant (p <0.001) later increase in cccDNA in the untreated cells (Fig. 2c, green symbols). Subsequently, the treatment parameters (ε, η, and Q) were fitted separately for ETV and ETV + Myr-preS1. For cells treated with Myr-preS1 alone, ε and η were set to 0 and 1, respectively.

Results

ETV treatment during infection initiation prevents amplification of exHBV levels

Four exHBV kinetic phases were identified in the untreated PHH cells (Fig. 2A). The first phase was a rapid decline with a slope of ~0.8 log/day ($t_{1/2}$ = 8.6 h) until Day 3 p.i. This was followed by a slow increase between Days 3 and 5 pi (phase 2 slope = 0.08 log/day). Thereafter, exHBV increased rapidly, with a slope of 0.43 log/day between Days 5 and 7 p.i. (phase 3), followed by a slower increase of 0.12 log/day from Day 7 onward (phase 4). The exHBV kinetic pattern was the same in untreated and Myr-preS1-treated samples (Fig. 2A, blue and red lines, respectively; Table S1.2). The kinetics of exHBV accumulation under the ETV (and ETV + Myr-preS1) treatment were similar through phase 2 but then diverged from the untreated and Myr-preS1 conditions, with exHBV levels remaining unchanged or slightly decreasing post phase 2 (Fig. 2A, purple and orange lines, respectively; Table S1.2). Similar kinetic trends were observed in independent experiment 2 (Fig. S1.1–S1.3) as well as with different human hepatocyte donors, HBV inoculation doses, or ETV concentrations (Fig. S1.4).

ETV treatment during infection initiation prevents amplification of inHBV levels

Four phases of inHBV from the time of inoculation in the untreated PHH cells were identified (Fig. 2B). All conditions exhibited a first phase inHBV decline. In untreated cells, the phase 1 slope was 0.32 log/day ($t_{1/2}$ = 22 h) until Day 2 p.i. This is followed by a roughly flat second phase until Day 5. In untreated and Myr-preS1-treated cultures, this was followed by a rapid increase from Days 5 to 7 (phase 3 slope = 0.29 log/day for untreated cells) and then a moderate increase from Days 7 to 12 (phase 4 slope = 0.08 log/day) (Fig. 2B, blue and red lines; Table S1.2). However, under the ETV treatment (with or without Myr-preS1), the phase 2 plateau was followed by a slow decline (phase 3 slope = -0.05 log/day for ETV alone) (Fig. 2B, purple and orange lines; Table S1.2). Similar kinetic patterns were observed in independent experiment 2 (Figs. S1.1–S1.3).

ETV treatment during infection initiation slows HBV cccDNA amplification but does not affect the plateau level

In the untreated PHH cells (Fig. 2C, blue line), there was a first-phase rapid increase until Day 2 p.i. (slope = ~0.96 log copies/well/day; $t_{1/2}$ = 8 h), followed by a slow phase 2 increase from Days 2 to 12 p.i. that was significantly (p = 1.4e-8) different from 0 (slope = 0.04 log/day). Under the Myr-preS1 treatment, the initial increase was followed by a plateau from Days 2 to 12, which was not significantly (p = 0.74) different from 0 (Fig.2C, red line). Under the ETV treatment, cccDNA increased in a biphasic pattern, first up to Day 2 at 0.51 log/day and then from Days 2 to 5 at a slower rate of 0.17 log/day (Fig. 2C, purple line). A similar pattern was observed with ETV + Myr-preS1-treated cultures (Fig. 2C, orange line). Similar kinetic trends were observed in independent experiment 2 (Figs. S1.1–S1.3). The plateau levels of cccDNA under the ETV, Myr-preS1, and ETV + Myr-preS1 treatments were identical.

Selecting the best mathematical model to reproduce the experimental data

We chose not to test our models using the data from untreated cultures because there was an increase in cccDNA later in the experiment, suggesting there may have been HBV spread (Fig. 2C, blue line). We therefore used Myr-preS1-treated cells for our baseline modeling to investigate initial HBV amplification kinetics without spread. Data from the cultures treated with ETV + Myr-preS1 and ETV alone, which were almost identical (Fig. 2), were also modeled to investigate the effect of ETV.

To replicate the kinetics of inHBV, exHBV, and cccDNA during early infection and ETV treatment in PHHs, we explored multiple models (Supplementary file, Section S2, Models S2.0–S2.4, Table S2.1), each consisting of three compartments: cccDNA (C) in the nucleus, total inHBV (V_i) in the cytoplasm, and exHBV (V_e) in the media. The key features in our final model (shown in Eqs 1–3) are as follows: (i) cccDNA production based on a self-dependent logistic growth rate function, (ii) a time-dependent synthesis rate of inHBV, (iii) recycling of encapsidated HBV DNA to the nucleus for the formation of cccDNA being dependent on inHBV levels, (iv) a secretion rate of inHBV that is dependent on its own concentration, and (v) a time dependence in the efficacy of ETV in blocking the production of inHBV (see Supplementary file, Section S2). The final model presented in Eqs 1–3 fits the experimental data well (Fig. 3), including the Myr-preS1 (Fig. 3A), ETV + Myr-preS1 (Fig. 3B), and ETV-alone treatments (Fig. 3C).

Estimating time for HBV to infect cells and begin cccDNA synthesis

If the model starts at the time of HBV inoculation (t = 0), good fits could not be obtained (not shown), consistent with the expectation that it takes time for the inoculated HBV to enter the cell, the DNA to be delivered to the nucleus, and cccDNA to

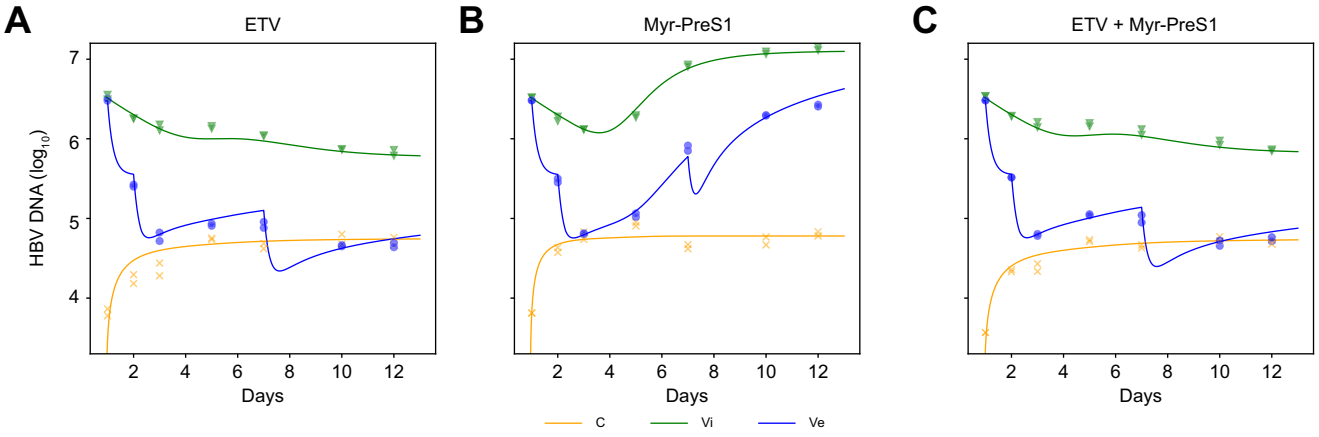

Fig. 3. HBV kinetics and model (Eqs 1–3) fit curves in PHHs treated with ETV and/or Myrcludex (Myr-preS1) for 12 days. (A) ETV-treated PHHs, (B) Myr-PreS1-treated PHHs, and (C) ETV + Myr-preS1-treated PHHs. There are three samples measured at each time point. Lines represent model best fits corresponding to Eqs 1–3. The beginning of cccDNA amplification after the time of HBV inoculation is estimated as 22 h (parameter S_0 in Table 1). The drop in extracellular HBV DNA at time points 1, 2, and 7 replicates the replenishment at Days 1, 2, and 7, respectively. Parameter values are shown in Table 1. Note that for (A) and (C), parameters S_0, σ_{max}, C_{max}, τ, p_{max}, κ_{max}, μ, ν, and τ_1 were fixed based on their values from (B). ETV, entecavir; Myr-preS1, myristoylated pre-S/2-48myr peptide; PHH, primary human hepatocyte.

Table 1. Parameter estimations.

Parameter definition (notation, unit)	Value ± SD	Figure(s) where value is used
Starting time of model integration (S_0, h)	22.1 ± 0.3	Fig. 3A–C
Maximum recycling rate constant (σ_{max}, per day)	0.029 ± 0.005	Fig. 3A–C
Maximum capacity of cccDNA (C_{max}, log10 cps)	4.79 ± 0.02	Fig. 3A–C
Time to reach the maximum level of inHBV production (τ, day)	5.05 ± 0.12	Fig. 3A–C
Maximum production rate of inHBV (p_{max}, per day)	116 ± 12	Fig. 3A–C
Maximum secretion rate of inHBV (κ_{max}, per day)	0.093 ± 0.009	Fig. 3A–C
Delay before secretion of inHBV (τ_1, day)	2.63*	Fig. 3A–C
Degradation rate constant of inHBV (μ, per day)	0.493 ± 0.048	Fig. 3A–C
Fraction of replenishment decay (ν)	0.926 ± 0.026	Fig. 3A–C
Efficacy of ETV alone in reducing accumulation of cccDNA (η)	0.48 ± 0.05	Fig. 3B
Total treatment inhibition of iHBV synthesis under ETV alone at Day 3	0.60 ± 0.04	Fig. 3B
Total treatment inhibition of iHBV synthesis under ETV alone at Day 5	0.78 ± 0.04	Fig. 3B
Total treatment inhibition of iHBV synthesis under ETV alone at Day 12	0.97 ± 0.02	Fig. 3B
Efficacy of ETV + Myr-preS1 in reducing accumulation of cccDNA (η)	0.394 ± 0.033	Fig. 3C
Total treatment inhibition of iHBV synthesis under ETV + Myr-preS1 at Day 3	0.65 ± 0.04	Fig. 3C
Total treatment inhibition of iHBV synthesis under ETV + Myr-preS1 at Day 3	0.82 ± 0.04	Fig. 3C
Total treatment inhibition of iHBV synthesis under ETV + Myr-preS1 at Day 3	0.97 ± 0.02	Fig. 3C

Fixed parameters were d_c = 0.1, ψ = 0.012, M = 1.5, V_{i50} = 5e6, and N = 1. *Uncertainty could not be estimated. cccDNA, covalently closed circular DNA; ETV, entecavir; exHBV, extracellular HBV DNA; inHBV, intracellular HBV DNA.

be formed. To address this, we incorporated a parameter into the model, defining the starting time point of productive HBV infection (S_0), which the model estimated to be 22.1 ± 0.3 h (Table 1 and Fig. 3).

Modelling suggests cccDNA accumulates according to a logistic growth function

To reproduce the observed cccDNA accumulation within the originally infected cells, we focused on the Myr-preS1-treated cultures (Fig. 3A) and found that the recycling of inHBV to cccDNA during initial infection follows a logistic growth function, where cccDNA accumulation stops above a certain level (Models S2.0 and 2.1 and Figs. S2.0 and S2.1). The maximum accumulation rate of cccDNA was found to be σ_{max} = 0.029 per day, and the maximum level of cccDNA was given by a capacity C_{max} = 4.79 ± 0.02 $\log_{10}$ cccDNA cps/well. Hence, after an S_0 delay of 22 h, the initial rate of cccDNA accumulation was 100,000 copies per day per well but then quickly decreased to less than half within 12 h, plateauing within 24 h (~2 days p.i.; Fig. 3A).

Production of inHBV ramps up over time

A fixed production rate cannot explain the observed inHBV kinetics (Model S2.0 and Fig. S2.0); instead, a time-dependent rate is needed (Model S2.1 and Fig. S2.1). Consistent with exponential viral amplification, there is a ramp-up in the production of inHBV, and the estimated time to reach 50% of the maximum production rate, p_{max}, is τ = 5.05 ± 0.12 days. At the maximum, each copy of cccDNA corresponds to an average production of p_{max} = 116 ± 12 inHBV per well per day. The clearance rate of inHBV was estimated to be μ = 0.493 ± 0.048 1/day, corresponding to a half-life of 34 ± 3 h.

Secretion rate of inHBV varies with its concentration

The model predicts that the secretion rate of HBV DNA is dependent on the concentration of inHBV with an initially estimated delay of 41 h after the start of cccDNA formation, which corresponds to τ_1 = 2.63 days p.i (Fig. S2.1 and Model S2.3). The HBV secretion rate then ramps up according to a Hill function with a maximum secretion rate of κ_{max} = 0.093 ± 0.009 per day. By Day 12, the number of inHBV copies secreted as virions reached 86,000 HBV cps/well/day.

Media removal and replenishment explain the early decline in exHBV

There was a decline in exHBV until Day 3 (Fig. 3A); however, exHBV proved to be very stable in media at 37 °C (Table S1.3), resulting in exHBV half-life being fixed at ~57 days, which cannot explain the 1.5 log decline in exHBV by Day 3. However, the virus was removed as a result of cell culture media changes. Therefore, media removal/replenishment was incorporated into the model, which led to an estimated ν = 92.6% reduction (1 log IU/ml) in exHBV concentration.

ETV blocks inHBV synthesis with a predicted secondary effect of reducing cccDNA recycling

After estimating the parameters under the Myr-preS1-alone treatment, we then fitted the model to the kinetic data from the ETV-treated cultures to quantify the antiviral effects. Because the kinetics of inhibition observed under the ETV-alone and ETV + Myr-preS1 treatments were nearly identical (Fig. 2A–C), the model-estimated parameter values for both conditions were also similar with overlapping CIs (Table 1). Therefore, for simplicity, reported here are the parameter values averaged across both ETV treatment conditions. By blocking the reverse transcription step of HBV genome amplification, ETV's efficacy (ε) in blocking inHBV accumulation changes over time, exhibiting a rapid increase in efficacy before reaching a final value (Model S2.4). The model estimates that the efficacy of ETV in blocking inHBV synthesis increased over time with a rate constant of Q = 0.34 ± 0.03 1/day, corresponding to inhibition of 62%, 81%, 92%, and 97% of inHBV at 3, 5, 8, and 12 days p.i. Consequently, the model also predicts that the downstream secreted exHBV levels are reduced proportionately and recycling of inHBV to cccDNA is reduced under ETV treatment (Model S2.2). However, the reduction in cccDNA levels is not directly proportionate; instead, under the ETV treatment, whether alone or with Myr-preS1 (Table 1), cccDNA recycling is reduced, on average, by η = 44% ± 7%.

Discussion

Here, we presented a unique sampling of exHBV, inHBV, and cccDNA during early HBV infection in PHHs. We performed a detailed kinetic characterization of each parameter and found that both untreated and Myr-preS1-treated PHHs had similar inHBV and exHBV kinetics, with both initially declining and then accumulating in a biphasic pattern. In contrast, PHHs treated with ETV exhibited a decline in both exHBV and inHBV without any resurgences. In contrast, cccDNA levels increased rapidly and quickly reached a plateau under all conditions, although untreated PHHs had a subsequent increase, which we hypothesize was because of spread. Although ETV-treated cultures had slower cccDNA accumulation, the final plateau level was similar to that of Myr-preS1-treated PHHs.

To better understand the early HBV kinetics, we developed a multicompartmental mathematical model that was able to accurately reproduce the kinetics of inHBV, exHBV, and cccDNA in Myr-preS1-treated cells. Notably, we incorporated model features from several prior studies such as a time dependence for inHBV production[27] and a Hill function to describe the secretion of inHBV.[28] We found herein that exHBV is stable in media yet observed an initial decline over 3 days. We accounted for this via media replenishment in the model. The model allowed an estimation of the time from inoculation to the start of cccDNA accumulation, which was found to be approximately 22 h. Only after approximately 3 days p.i. did we observe an increase in exHBV similar to the slow infection kinetics reported by Ko *et al.*[10] in a selected HepG2 cell clone expressing NTCP. This also suggests that the eclipse phase could be between 22 and 72 h, reminiscent of previous eclipse phase estimates in humanized mice.[27]

For ETV-based treatments, simultaneous fits of the multicompartment mathematical model to inHBV, exHBV, and cccDNA predicted a high level of blocking of inHBV accumulation with a maximum ETV efficacy of 97%, explaining the lack of inHBV and exHBV resurgence. In addition, the model predicted that ETV slowed cccDNA accumulation during early infection within the cell by 44% (*i.e.* before the steady state) without affecting the final cccDNA plateau level. It is important to emphasize that the effects of ETV on cccDNA dynamics during early infection in PHH reveal that cccDNA accumulation is not simply or directly related to total inHBV levels. We recently hypothesized, based on HBV RNA kinetics, that NAs may have multifunctional antiviral effects, such as potential transcriptional inactivation or degradation of cccDNA,[29] which could explain the observed effect of slowing cccDNA accumulation in the present study. Nonetheless, whether the effects on cccDNA accumulation reflect a currently unknown mechanism regulating cccDNA recycling or an unexpected secondary effect of NAs remains to be determined.

Meanwhile, this study has several potential limitations that should be noted. First, although additional experiments with different batches of PHHs from different PHH donors, different HBV inoculations, and ETV doses showed similar exHBV kinetic patterns (Fig. S1.4), the results and modeling efforts presented here were performed with one particular batch of PHHs. Additional analysis should be performed, measuring not only exHBV but also cccDNA and inHBV to determine how different HBV genotypes, inoculation sizes, and PHH batches affect the kinetics and confirm that the model can recapitulate these data. Third, although the accuracy of cccDNA quantification is dependent on the ratio of cccDNA to relaxed circular DNA,[30] and this ratio was within the range where cccDNA concentration is considered accurate (below 250) for most time points, this was not the case on Day 1, making our quantification of cccDNA on Day 1 potentially less accurate. Fourth, we excluded data measured in untreated cells from modeling because we believe the later increase in cccDNA, which was significantly ($p<0001$) higher at Day 12 than in the treated cells, resulted from spread. Although we cannot be certain because infected cell numbers were not measured, a recent publication that did measure infected cell numbers found that untreated PHHs do have considerably more infected cells than Myr-preS1-treated PHHs.[31] Lastly, although the viral kinetics and modeling presented here indicate that cccDNA levels are not simply a direct result of relaxed circular DNA levels, our study does not provide any insight regarding the viral factors that determine the maximal level of cccDNA in an infected hepatocyte, which remains an important open question.

In summary, mathematical modeling confirms that ETV strongly blocks the synthesis of inHBV accumulation in PXB PHHs and demonstrates a nonproportional/nonlinear relationship between inHBV and cccDNA. These results may suggest a more complex regulation of cccDNA accumulation, which requires further investigation.

Affiliations

[1]*The Program for Experimental and Theoretical Modeling, Division of Hepatology, Department of Medicine, Loyola University Medical Center, Maywood, IL, USA;* [2]*Department of Information Science, Bar-Ilan University, Ramat Gan, Israel;* [3]*PhoenixBio Co., Ltd., Higashi-Hiroshima, Japan;* [4]*Liver Center, Hiroshima University Hospital, Hiroshima, Japan;* [5]*Department of Gastroenterology, Graduate School of Biomedical and Health Sciences, Hiroshima University, Hiroshima, Japan;* [6]*Department of Computer Science, Université du Québec à Montréal, Montréal, QC, Canada;* [7]*Hiroshima Institute of Life Sciences, Hiroshima, Japan;* [8]*RIKEN Center for Integrative Medical Sciences, Yokohama, Japan*

Abbreviations

cccDNA, covalently closed circular DNA; ETV, entecavir; exHBV, extracellular HBV DNA; GEg, genome equivalents; inHBV, intracellular HBV DNA; Myr-preS1, myristoylated pre-S/2-48myr peptide; p.i., post inoculation; PEG, polyethylene glycol; PHH, primary human hepatocyte; qPCR, quantitative real-time PCR.

Financial support

The study was supported in part by Japan Agency for Medical Research and Development (AMED) under grant 19fk0210020h0003, the Fund for the Promotion of Joint International Research (Fostering Joint International Research) from Japan Society for the Promotion of Science (grant number 17KK0194), Binational Science Foundation grant number 207745, and US NIH grants R01AI144112 and R01AI146917. The funders had no role in study design, data collection and analysis, decision to publish, or preparation of the manuscript.

Conflicts of interest

YI, MY, MTa, and CT are PhoenixBio employees. All other authors have nothing to disclose.

Please refer to the accompanying ICMJE disclosure forms for further details.

Authors' contributions

Concept and design: HD, KC. Experimental (*in vitro*) data: YI, MY, MTa, CT, KC. In silico modeling: LS, VR, HD. Visualization: LS. Writing of the manuscript: LS, YI, MTs, SLU, HD, KC. Supervision: KC, HD. Funding acquisition: SLU, HD, KC. Reviewed and approved the final version of the manuscript: all authors.

Data availability statement

Data is available on request from the authors.

Acknowledgments

We thank Preeti Dubey for initial kinetic and theoretical modeling analyses.

Supplementary data

Supplementary data to this article can be found online at https://doi.org/10.1016/j.jhepr.2024.101311.

References

Author names in bold designate shared co-first authorship

[1] World Health Organization, 2024. Hepatitis B. Key Facts. https://www.who.int/news-room/fact-sheets/detail/hepatitis-b. [Accessed 28 January 2025].
[2] Ligat G, Goto K, Verrier E, et al. Targeting viral cccDNA for cure of chronic hepatitis B. Curr Hepatol Rep 2020;19:235–244.
[3] Fung S, Choi HS, Gehring A, et al. Getting to HBV cure: the promising paths forward. Hepatology 2022;76:233–250.
[4] **Petersen J**, **Dandri M**, Mier W, et al. Prevention of hepatitis B virus infection in vivo by entry inhibitors derived from the large envelope protein. Nat Biotechnol 2008;26:335–341.
[5] **Volz T**, **Allweiss L**, Ḿbarek MB, et al. The entry inhibitor Myrcludex-B efficiently blocks intrahepatic virus spreading in humanized mice previously infected with hepatitis B virus. J Hepatol 2013;58:861–867.
[6] Allweiss L, Volz T, Giersch K, et al. Proliferation of primary human hepatocytes and prevention of hepatitis B virus reinfection efficiently deplete nuclear cccDNA in vivo. Gut 2018;67:542–552.
[7] Woo G, Tomlinson G, Nishikawa Y, et al. Tenofovir and entecavir are the most effective antiviral agents for chronic hepatitis B: a systematic review and Bayesian meta-analyses. Gastroenterology 2010;139:1218–1229. e5.
[8] Yokosuka O, Takaguchi K, Fujioka S, et al. Long-term use of entecavir in nucleoside-naive Japanese patients with chronic hepatitis B infection. J Hepatol 2010;52:791–799.
[9] Bowden S, Locarnini S, Chang T-T, et al. Covalently closed-circular hepatitis B virus DNA reduction with entecavir or lamivudine. World J Gastroenterol 2015;21:4644–4651.
[10] Ko C, Chakraborty A, Chou WM, et al. Hepatitis B virus genome recycling and de novo secondary infection events maintain stable cccDNA levels. J Hepatol 2018;69:1231–1241.
[11] Murray JM, Wieland SF, Purcell RH, et al. Dynamics of hepatitis B virus clearance in chimpanzees. Proc Natl Acad Sci U S A 2005;102:17780–17785.
[12] Murray JM, Goyal A. In silico single cell dynamics of hepatitis B virus infection and clearance. J Theor Biol 2015;366:91–102.
[13] Goyal A, Chauhan R. The dynamics of integration, viral suppression and cell–cell transmission in the development of occult Hepatitis B virus infection. J Theor Biol 2018;455:269–280.
[14] Kitagawa K, Kim KS, Iwamoto M, et al. Multiscale modeling of HBV infection integrating intra-and intercellular viral propagation to analyze extracellular viral markers. Plos Comput Biol 2024;20:e1011238.
[15] **Ishida Y**, **Chung TL**, Imamura M, et al. Acute hepatitis B virus infection in humanized chimeric mice has multiphasic viral kinetics. Hepatology 2018;68:473–484.
[16] Kohara H, Bajaj P, Yamanaka K, et al. High-throughput screening to evaluate inhibition of bile acid transporters using human hepatocytes isolated from chimeric mice. Toxicol Sci 2020;173:347–361.
[17] Yamasaki C, Ishida Y, Yanagi A, et al. Culture density contributes to hepatic functions of fresh human hepatocytes isolated from chimeric mice with humanized livers: novel, long-term, functional two-dimensional in vitro tool for developing new drugs. PLoS One 2020;15:e0237809.
[18] Tateno C, Miya F, Wake K, et al. Morphological and microarray analyses of human hepatocytes from xenogeneic host livers. Lab Invest 2013;93:54–71.
[19] Ishida Y, Yamasaki C, Yanagi A, et al. Novel robust in vitro hepatitis B virus infection model using fresh human hepatocytes isolated from humanized mice. Am J Pathol 2015;185:1275–1285.
[20] Abe A, Inoue K, Tanaka T, et al. Quantitation of hepatitis B virus genomic DNA by real-time detection PCR. J Clin Microbiol 1999;37:2899–2903.
[21] Takkenberg R, Zaaijer H, Molenkamp R, et al. Validation of a sensitive and specific real-time PCR for detection and quantitation of hepatitis B virus covalently closed circular DNA in plasma of chronic hepatitis B patients. J Med Virol 2009;81:988–995.
[22] Watashi K, Liang G, Iwamoto M, et al. Interleukin-1 and tumor necrosis factor-α trigger restriction of hepatitis B virus infection via a cytidine deaminase activation-induced cytidine deaminase (AID). J Biol Chem 2013;288:31715–31727.
[23] Köck J, Rösler C, Zhang J-J, et al. Generation of covalently closed circular DNA of hepatitis B viruses via intracellular recycling is regulated in a virus specific manner. Plos Pathog 2010;6:e1001082.
[24] Peters MG, Locarnini S. New direct-acting antiviral agents and immunomodulators for hepatitis B virus infection. Gastroenterol Hepatol 2017;13:348–356.
[25] Virtanen P, Gommers R, Oliphant TE, et al. SciPy 1.0: fundamental algorithms for scientific computing in Python. Nat Methods 2020;17:261–272.
[26] Newville M, Stensitzki T, Allen DB, *et al.* LMFIT: non-linear least-square minimization and curve-fitting for Python. Astrophysics Source Code Libr 2016:ascl:1606.014.
[27] **Hailegiorgis A**, **Ishida Y**, Collier N, et al. Modeling suggests that virion production cycles within individual cells is key to understanding acute hepatitis B virus infection kinetics. Plos Comput Biol 2023;19:e1011309.
[28] **Reiharz V**, **Ishida Y**, Tsuge M, et al. Understanding hepatitis B virus dynamics and the antiviral effect of interferon alpha treatment in humanized chimeric mice. J Virol 2021;95:e0049220.
[29] Dahari H, Vaillant A, Cotler SJ. Letter to the editor: examining HBV-RNA kinetics during NA treatment—are NAs multifunctional antiviral agents? Hepatology 2021;74:1708–1709.
[30] Allweiss L, Testoni B, Yu M, et al. Quantification of the hepatitis B virus cccDNA: evidence-based guidelines for monitoring the key obstacle of HBV cure. Gut 2023;72:972–983.
[31] Shi Z, Tsuge M, Collier N, et al. Modeling of hepatitis B virus infection spread in primary human hepatocytes. bioRxiv 2025. https://doi.org/10.1101/2025.02.05.636596.

Keywords: HBV; cccDNA; Mathematical modeling; Primary human hepatocytes; Entecavir; Entry inhibitor.

Received 5 November 2024; received in revised form 11 December 2024; accepted 16 December 2024; Available online 24 December 2024